Single Top Production at Next-to-Leading Order in the Standard Model Effective Field Theory

Cen Zhang
Department of Physics, Brookhaven National Laboratory, Upton, New York 11973, USA
(Received 28 January 2016; published 21 April 2016)

Single top production processes at hadron colliders provide information on the relation between the top quark and the electroweak sector of the standard model. We compute the next-to-leading order QCD corrections to the three main production channels: t-channel, s-channel, and tW associated production, in the standard model including operators up to dimension six. The calculation can be matched to parton shower programs and can therefore be directly used in experimental analyses. The QCD corrections are found to significantly impact the extraction of the current limits on the operators, because both of an improved accuracy and a better precision of the theoretical predictions. In addition, the distributions of some of the key discriminating observables are modified in a nontrivial way, which could change the interpretation of measurements in terms of UV complete models.

DOI: 10.1103/PhysRevLett.116.162002

Introduction.—At high-energy colliders, physics beyond the standard model (SM) is searched for either by looking for evidence of new particles or for deviations in the predicted interactions between the SM particles. In the latter effort the top quark plays a special role: thanks to its large mass it can naturally probe high scales and in particular the electroweak symmetry breaking sector. A general theoretical framework where the experimental information on the interactions and possible deviations can be consistently and systematically interpreted is provided by the SM effective field theory (SMEFT) approach [1–3]. The SMEFT Lagrangian corresponds to that of the SM augmented by higher-dimensional operators that respect the symmetries of the SM. It provides a powerful approach to identify observables where deviations could be expected in the top sector [4–6]. Besides, and more importantly, it allows a global interpretation of measurements coming from different processes and experiments [7–10], which can be consistently evolved up to new physics scales, and provide hints to specific models at high scales.

Given the results of the LHC run I [11], expectations from run II on the attainable precision of the top-quark couplings are very high. Theoretical predictions that are at least as accurate and precise as the experimental projections are thus required. This motivates the calculation of higher-order corrections. In this work, we focus on the single-top production processes. At the LHC, single-top production proceeds through three main channels: the t channel, s channel, and tW associated production. They are ideal for probing the top-quark couplings to the electroweak sector of the SM, and can provide key and complementary information to that coming from top-quark decay. To this aim we promote the single-top predictions, for the first time, to next-to-leading order (NLO) in QCD in the SMEFT, and study their impact on the interpretation of measurements.

The main results of this work can be summarized as follows. First, we show that QCD corrections not only affect total cross sections and reduce their uncertainties, but also impact the distributions of key observables, in such a way that the interpretation of possible deviations from the SM would lead to quite different UV complete models. Moreover, these corrections cannot be captured by either the K factors or the renormalization group (RG) improvements of the Wilson coefficients. Second, we demonstrate that a new type of scale uncertainty in EFT, coming from the running and mixing of dimension-six terms, needs to be considered and can be reduced by including QCD corrections. Finally, by matching our NLO computation to a parton shower (PS) program, predictions can be obtained through an event generator that can be used directly in experimental simulations, to design optimized analyses that can maximize the sensitivity to new physics.

Effective operators.—In the EFT approach deviations from the SM are captured by effective operators. Up to dimension six, four operators are relevant [4,5,12]:

$$O_{\varphi Q}^{(3)} = i\frac{1}{2}y_t^2(\varphi^\dagger \overleftrightarrow{D}_\mu^I \varphi)(\bar{Q}\gamma^\mu \tau^I Q), \tag{1}$$

$$O_{tW} = y_t g_W (\bar{Q}\sigma^{\mu\nu}\tau^I t)\tilde{\varphi} W_{\mu\nu}^I, \tag{2}$$

$$O_{tG} = y_t g_s (\bar{Q}\sigma^{\mu\nu}T^A t)\tilde{\varphi} G_{\mu\nu}^A, \tag{3}$$

$$O_{qQ,rs}^{(3)} = (\bar{q}_r\gamma_\mu\tau^I q_s)(\bar{Q}\gamma^\mu\tau^I Q). \tag{4}$$

Here q_r and q_s are the quark doublet fields in the first two generations, while Q is in the third generation. r, s are flavor indices. φ is the Higgs doublet. g_W, g_Y, and g_s are the SM gauge coupling constants. y_t is the top-quark Yukawa coupling, defined by its pole mass. The effective Lagrangian is

$$\mathcal{L}_{\text{eff}} = \mathcal{L}_{\text{SM}} + \sum_i \frac{C_i}{\Lambda^2} O_i + \text{H.c.}, \tag{5}$$

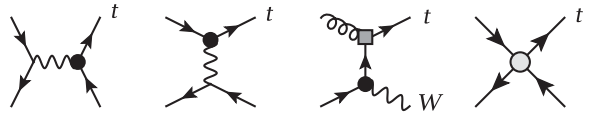

FIG. 1. Representative leading order (LO) diagrams for all three single-top channels. Vertices with a black dot can be modified by $O_{\phi Q}^{(3)}$ and O_{tW}, while that with a square is modified by O_{tG}. The last diagram comes from $O_{qQ}^{(3)}$.

where Λ is the expected scale of new physics. C_i is the coefficient to parametrize the deviation from O_i. In this work we assume flavor universality in the first two generations, defining $O_{qQ}^{(3)} = O_{qQ,11}^{(3)} + O_{qQ,22}^{(3)}$. Dimension-six operators affect all three channels. Corresponding diagrams are shown in Fig. 1.

The operators O_{tG} and O_{tW} have nonzero anomalous dimensions at $\mathcal{O}(\alpha_s)$, given by [13–16]

$$\frac{dC_i}{d\log\mu} = \frac{\alpha_s}{\pi}\gamma_{ij}C_j, \quad \gamma = \frac{1}{3}\begin{pmatrix} 1 & 0 \\ 2 & 2 \end{pmatrix}. \tag{6}$$

This matrix controls the running and mixing of the operators and can be used to evolve them from scale Λ down to the scales of the measurements.

Calculation.—The NLO automation is implemented and validated in the MadGraph5_aMC@NLO framework [17], with the help of a series of packages, including FeynRules and NLOCT [18–24]. A model in the Universal FeynRules Output format [20] is built at NLO, allowing for the simulation of a variety of processes important for top-coupling measurements. In this work we only focus on single-top processes, but other promising (and more complicated) channels, such as $t\bar{t}Z/W/\gamma$ and tjZ/γ, are all made available at NLO in EFT with PS. In Ref. [25] we have discussed the physical results for $t\bar{t}Z/W/\gamma$ processes. More details of this implementation will be presented in a separate work [26].

We adopt $\overline{\text{MS}}$ with five-flavor running in α_s with the top-quark subtracted at zero momentum transfer [27]. Additional contributions to top-quark and gluon-field renormalizations and α_s renormalization from O_{tG} are included [28]. For operator coefficients we use $\overline{\text{MS}}$ subtraction, with

$$C_i^0 \to Z_{ij}C_j(\mu') = \left[\mathbb{1} + \frac{\alpha_s}{2\pi}\Gamma(1+\varepsilon)\left(\frac{4\pi\mu^2}{\mu'^2}\right)^{\varepsilon}\frac{1}{\varepsilon_{\text{UV}}}\gamma\right]_{ij} C_j(\mu') \tag{7}$$

where the anomalous dimension matrix γ is given in Eq. (6). UV counterterms needed in this work are computed using the above information. Note that with Eq. (7) the operators will run with μ' separately from the running of α_s. This allows for the dynamical renormalization scale to be adopted without having to run the operator coefficients.

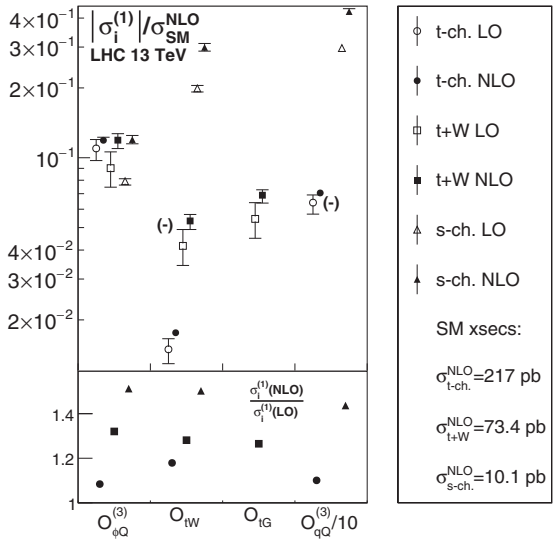

FIG. 2. $r_i = |\sigma_i^{(1)}|/\sigma_{\text{SM}}^{\text{NLO}}$ for the three single-top channels. Both LO and NLO results are shown. Error bars indicate scale uncertainties. K factors are given in the lower panel. Negative contributions are labeled with "(−)."

Results are presented in terms of operators defined at $\mu' = m_t$, i.e., the log terms from high scale, $\log(\Lambda/m_t)$, are already resummed by evolving operators down to this scale using Eq. (6). Thus the NLO corrections presented here do not include any of such large log terms, and *cannot* be captured by the RG equations.

Total cross sections.—Cross sections, obtained at LO and NLO, can be parametrized as

$$\sigma = \sigma_{\text{SM}} + \sum_i \frac{1\ \text{TeV}^2}{\Lambda^2} C_i\sigma_i^{(1)} + \sum_{i\le j} \frac{1\ \text{TeV}^4}{\Lambda^4} C_iC_j\sigma_{ij}^{(2)} + \cdots$$

We work up to order $1/\Lambda^2$, and present results for $\sigma_i^{(1)}$, the interference between an operator O_i and the SM. We use NNPDF2.3 parton distributions [29]. Input parameters are

$$m_t = 172.5\ \text{GeV}, \qquad m_Z = 91.1876\ \text{GeV}, \tag{8}$$

$$\alpha(m_Z) = 1/127.9, \quad G_F = 1.16637\times10^{-5}\ \text{GeV}^{-2}. \tag{9}$$

Central renormalization and factorization scales are fixed at $\mu_R = \mu_F = m_t$. To estimate theoretical uncertainties due to missing higher orders we perform variations with nine combinations of (μ_R, μ_F), where $\mu_{R,F}$ can take values $m_t/2$, m_t and $2m_t$.

Total cross sections (including top and antitop) at LHC 13 TeV are presented in Figure 2. We plot the ratio between the interference cross section, $\sigma_i^{(1)}$, and SM NLO cross section, $r_i = |\sigma_i^{(1)}|/\sigma_{\text{SM}}^{\text{NLO}}$, for individual operators O_i, in all three channels. The ratio r_i illustrates how sensitive a process is to a certain operator, and can be interpreted as the signal over background ratio. In the plot, scale uncertainties from the numerator are given, and in the lower panel we show the K factor of each operator contribution. Improved accuracy is

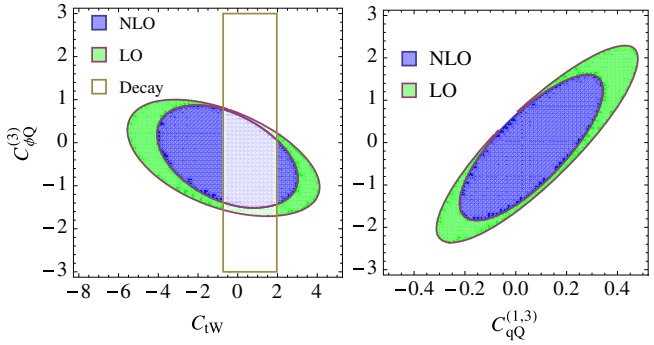

FIG. 3. 95% limit from single-top measurements, with LO or NLO predictions for EFT. Left: $(O^{(3)}_{\phi Q}, O_{tW})$; right: $(O^{(3)}_{\phi Q}, O^{(3)}_{qQ})$. Limits from top decay measurements are compared.

reflected by the K factors, typically ranging from ∼10% to ∼50%, and improved precision is reflected by the significantly reduced scale uncertainties. Furthermore, most NLO results are outside of the uncertainty range of corresponding LO results, indicating that QCD corrections are essential for a correct interpretation of measurements in terms of operators. For comparison, at 8 TeV the t channel has been measured at better than ∼10% level [30,31], and the $t+W$ channel is at about 20% [32]. At the high-luminosity LHC the t channel can reach ∼4% [33], while the s channel may reach ∼15% [34]. NNLO approximate QCD corrections are available for the SM predictions, and corresponding theoretical uncertainties are at the percentage level [35].

NLO corrections already affect current bounds on the coefficients of the dimension-six operators. For illustration we perform two-operator fits, for $(O^{(3)}_{\phi Q}, O_{tW})$ and for $(O^{(3)}_{\phi Q}, O^{(3)}_{qQ})$, using cross sections available at the LHC at 8 TeV [30–32,36] with the state-of-the-art SM prediction [35] and NLO EFT predictions from this work. Limits are improved thanks to better accuracy and precision, and can be clearly seen in Fig. 3. For comparison we also show current limits on O_{tW} from decay measurements [16,37,38]. (See also Ref. [39] for RG-induced bounds on top-quark operators.)

Distributions.—The QCD corrections have more crucial effects on the shapes of observables that can be used to identify deviations. Some key observables have very distinct distributions that depend on the relative contribution from different operators. If any deviation in the total cross section is observed, these observables will determine which operator is the source of the deviation. Even without any deviation, including these observables in a global analysis can help to constrain flat directions.

In our approach, distributions can be obtained at NLO in QCD with PS simulation [24,40], and with top quarks decayed, keeping spin correlations [41]. In Fig. 4 we show the normalized distributions of the top-quark rapidity, y_t, in t-channel single-top production, which is an efficient discriminating observable, and has been measured already

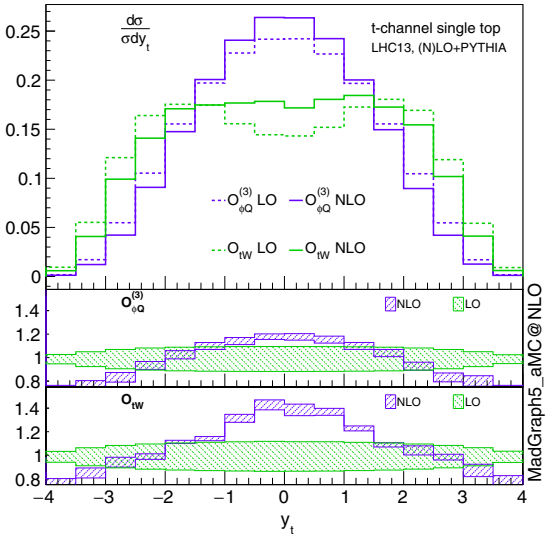

FIG. 4. Normalized rapidity distributions of the top quark in t-channel single-top production, from O_{tW} and $O^{(3)}_{\phi Q}$. Only the interference with the SM is included. Lower panel shows the K factors of individual operators, with scale uncertainties.

[42,43]. We can see that its distribution is more forward for O_{tW} while rather central for $O^{(3)}_{\phi Q}$. The difference arises already at the parton level due to the Lorentz structure of O_{tW} suppressing the forward scattering amplitude [5], and it is diluted at NLO due to real corrections.

Figure 4 also explains why NLO corrections are important when shape information is used. It makes both distributions more central, and missing this correction would lead to an underestimate of the size of the O_{tW} contribution on one hand and a corresponding overestimate of $O^{(3)}_{\phi Q}$ on the other. We find that other variables, including p_T and rapidity of the first non-b jet and of the first b jet, are affected in a similar way. Moreover, the theory uncertainty in shapes due to missing QCD is not captured by varying μ_R and μ_F. We thus conclude that NLO QCD corrections can lead to bias in an EFT analysis, by shifting the theoretical predictions for the shapes of discriminating observables.

To quantify this effect, we consider two benchmark points, (1): $C^{(3)}_{\phi Q} = 0.8$, $C_{tW} = 2$, and (2): $C^{(3)}_{\phi Q} = -1.1$, $C_{tW} = -1.4$, each corresponding to about a 15% deviation in the total cross section. We compute at NLO the distributions of two observables, y_t and p_T of the first non-b jet, and use the results as pseudodata, which we consider in 5 bins for $p_{T,j}$ from 20 to 180 GeV and 6 bins for $|y_t|$ from 0 to 3. We then perform χ^2 fits with LO and NLO predictions, respectively, and compare. Results depend on the combined uncertainty of experiment and theory. Current data at LHC 8 TeV correspond to ∼10% uncertainty in each bin [43]. Foreseeing future improvements in the analyses, we assume ∼5% uncertainty in each

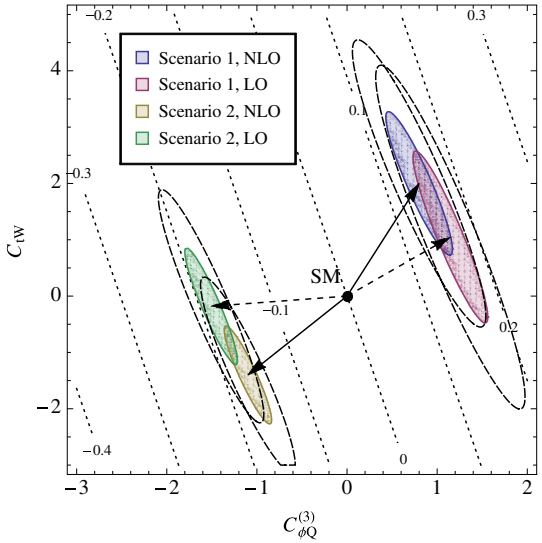

FIG. 5. Two-operator fit using pseudomeasurements on shapes, at 68% confidence level, assuming 5% uncertainty in each bin. Dashed lines correspond to twice this uncertainty, while dotted contours are the relative deviation in total cross section.

bin and we find that the operator coefficients extracted from the fit are shifted by NLO effects. This is shown in Fig. 5.

The dotted contours in Fig. 5 represent a constant deviation in the cross section. Cross section measurements constrain the direction orthogonal to these contours. On the other hand, including shape information constrains the direction along these lines. The bias induced by QCD corrections is reflected by the dashed and the solid arrows, which represent the resulting deviations from the fit, at LO and NLO, respectively. For example, in the second scenario the central values of coefficients extracted at LO are $(-1.5, -0.18)$, and become $(-1.1, -1.4)$ at NLO, and the one-sigma regions have almost no overlap. This shift is not in the radial direction corresponding to an overall rescale by the NLO K factor. Rather, it leads to a different direction of deviation in the $C^{(3)}_{\phi Q} - C_{tW}$ plane, as clearly indicated by the angle between the dashed and the solid arrows.

At this point it is important to note that the two operators, $O^{(3)}_{\phi Q}$ and O_{tW}, correspond to different types of new physics [44]. The first operator is likely to be generated by mixing SM particles with heavy objects such as W' [45,46] and heavy quarks [47,48]; the second one is loop induced, and typical scenarios include two-Higgs-doublet models [49] and supersymmetric models [50–52]. It follows that a missing QCD correction will lead us to an incorrect conclusion about the type of UV physics.

To sum up, there are two kinds of QCD NLO effects for single-top processes. The first is on total cross sections. It can be captured by applying a K factor to LO results, and only affects the magnitude of deviation from the SM. The second is on the shapes of discriminator observables. It *cannot* be captured by a simple K factor, and it affects the

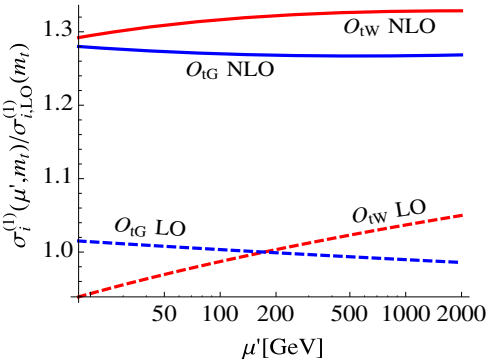

FIG. 6. The μ' dependence of $\sigma^{(1)}_{tW}(\mu', m_t)$ and $\sigma^{(1)}_{tG}(\mu', m_t)$ in tW production, normalized with $\sigma^{(1)}_{tW,tG}(\mu' = m_t)$ at LO. The dashed (solid) lines correspond to LO (NLO) calculation with one-loop running and mixing.

direction in which new physics deviates from the SM. Hence it is important because if deviations are observed in the single-top channel, missing such corrections would lead us to misinterpret measurements of possible deviations and misconclude the nature of UV physics.

EFT scale uncertainties.—Perturbative calculations performed in SMEFT suffer from a new source of scale uncertainty: the running and mixing of operator coefficients. In our calculation operators are defined at a scale μ', separately from $\mu_{R,F}$. This allows us to study this uncertainty alone, independent of the usual renormalization and factorization scale uncertainties.

This uncertainty can be estimated with $\sigma_i^{(1)}(\mu', \mu'_0) \equiv \Gamma(\mu', \mu'_0)_{ji}\sigma_j^{(1)}(\mu')$; i.e., the operator contributions at μ' evolved back to central scale μ'_0. Here Γ_{ij} is the solution to the RG equations:

$$\Gamma_{ij}(\mu', \mu'_0) = \exp\left(\frac{-2}{\beta_0}\log\frac{\alpha_s(\mu')}{\alpha_s(\mu'_0)}\gamma_{ij}\right), \qquad (10)$$

with $\beta_0 = 11 - 2/3n_f$, and $n_f = 5$ is the number of running flavors.

For illustration, we present the scale variation in the tW associated channel. This process involves both O_{tW} and O_{tG} already at the tree level, so both the running and the mixing effects are observable. In Fig. 6 we show the μ' dependence of the dimension-six contribution from O_{tW} and O_{tG}, where we choose $\mu'_0 = m_t$ as the central scale, and vary μ' from $m_t/10$ to 2 TeV, fixing μ_R and μ_F. It is clear from the plot that this kind of scale dependence can be reduced at NLO, indicating that the leading QCD log terms from the running and mixing of operator coefficients are cancelled by NLO corrections. We should point out that there are cases where mixing effects are much more important than the presented example in Fig. 6 [15,39,53–60], but the latter is a proof of principle that the related EFT scale uncertainties can be taken under control by including the full NLO corrections.

Finally, it is worth pointing out that the RG equations for operators cannot capture the dominant NLO corrections. From the plot we can see that the RG correction to O_{tW} from high scale Λ down is negative, while the complete NLO correction gives a sizeable increase. A reliable result can only be obtained by carrying out the complete NLO computation. A similar observation in the context of Higgs physics has been pointed out by the authors of Refs. [61,62].

Summary.—We have presented predictions for single-top processes at NLO with PS in SMEFT. Bounds on higher-dimensional operators are improved thanks to better accuracy and precision. More importantly, QCD corrections lead to nontrivial modifications to the shapes of the most powerful discriminating observables. If new physics shows up in single-top processes, missing such corrections would change the interpretation of the measurements and lead us to bias our interpretations in terms of new physics models. We have also demonstrated that the scale uncertainties associated with the running and mixing of operator coefficients should be considered, and can be reduced by including NLO corrections.

Our results should be used in experimental simulations, as they are important for interpreting measurements, and are available as an NLO + PS event generator. With more accurate and precise EFT simulation and uncertainties under control, SM deviations can now be analyzed in a top-down way, designing new analyses to maximize sensitivity and allowing for a more efficient approach to the study of the top-quark interactions.

I am grateful for valuable discussions with S. Dawson and M. Selvaggi. This work is supported by U.S. Department of Energy under Grant No. DE-SC0012704.

[1] S. Weinberg, Phenomenological Lagrangians, Physica (Amsterdam) **96A**, 327 (1979).

[2] W. Buchmuller and D. Wyler, Effective Lagrangian analysis of new interactions and flavor conservation, Nucl. Phys. **B268**, 621 (1986).

[3] C. N. Leung, S. T. Love, and S. Rao, Low-energy manifestations of a new interaction scale: Operator analysis, Z. Phys. C **31**, 433 (1986).

[4] Q.-H. Cao, J. Wudka, and C. P. Yuan, Search for new physics via single top production at the LHC, Phys. Lett. B **658**, 50 (2007).

[5] C. Zhang and S. Willenbrock, Effective-field-theory approach to top-quark production and decay, Phys. Rev. D **83**, 034006 (2011).

[6] C. Degrande, J.-M. Gerard, C. Grojean, F. Maltoni, and G. Servant, Non-resonant new physics in top pair production at hadron colliders, J. High Energy Phys. 03 (2011) 125.

[7] C. Zhang, N. Greiner, and S. Willenbrock, Constraints on non-standard top quark couplings, Phys. Rev. D **86**, 014024 (2012).

[8] G. Durieux, F. Maltoni, and C. Zhang, Global approach to top-quark flavor-changing interactions, Phys. Rev. D **91**, 074017 (2015).

[9] A. Buckley, C. Englert, J. Ferrando, D. J. Miller, L. Moore, M. Russell, and C. D. White, Global fit of top quark effective theory to data, Phys. Rev. D **92**, 091501 (2015).

[10] A. Buckley, C. Englert, J. Ferrando, D. J. Miller, L. Moore, M. Russell, and C. D. White, Constraining top quark effective theory in the LHC run II era, arXiv:1512.03360.

[11] K. A. Olive *et al.* (Particle Data Group), Review of particle physics, Chin. Phys. **C38**, 090001 (2014).

[12] J. A. Aguilar-Saavedra, A Minimal set of top anomalous couplings, Nucl. Phys. **B812**, 181 (2009).

[13] E. E. Jenkins, A. V. Manohar, and M. Trott, Renormalization group evolution of the standard model dimension six operators I: Formalism and lambda dependence, J. High Energy Phys. 10 (2013) 087.

[14] E. E. Jenkins, A. V. Manohar, and M. Trott, Renormalization group evolution of the standard model dimension six operators II: Yukawa dependence, J. High Energy Phys. 01 (2014) 035.

[15] R. Alonso, E. E. Jenkins, A. V. Manohar, and M. Trott, Renormalization group evolution of the standard model dimension six operators III: Gauge coupling dependence and phenomenology, J. High Energy Phys. 04 (2014) 159 (2014).

[16] C. Zhang, Effective Field Theory Approach to Top-Quark Decay at Next-to-Leading Order in QCD, Phys. Rev. D **90**, 014008 (2014).

[17] J. Alwall, R. Frederix, S. Frixione, V. Hirschi, F. Maltoni, O. Mattelaer, H.-S. Shao, T. Stelzer, P. Torrielli, and M. Zaro, The automated computation of tree-level and next-to-leading order differential cross sections, and their matching to parton shower simulations, J. High Energy Phys. 07 (2014) 079.

[18] A. Alloul, N. D. Christensen, C. Degrande, C. Duhr, and B. Fuks, FeynRules 2.0—A complete toolbox for tree-level phenomenology, Comput. Phys. Commun. **185**, 2250 (2014).

[19] C. Degrande, Automatic evaluation of UV and R2 terms for beyond the Standard Model Lagrangians: A proof-of-principle, Comput. Phys. Commun. **197**, 239 (2015).

[20] C. Degrande, C. Duhr, B. Fuks, D. Grellscheid, O. Mattelaer, and T. Reiter, UFO—The Universal FeynRules output, Comput. Phys. Commun. **183**, 1201 (2012).

[21] P. de Aquino, W. Link, F. Maltoni, O. Mattelaer, and T. Stelzer, ALOHA: Automatic libraries of helicity amplitudes for Feynman diagram computations, Comput. Phys. Commun. **183**, 2254 (2012).

[22] V. Hirschi, R. Frederix, S. Frixione, M. V. Garzelli, F. Maltoni, and R. Pittau, Automation of one-loop QCD corrections, J. High Energy Phys. 05 (2011) 044.

[23] R. Frederix, S. Frixione, F. Maltoni, and T. Stelzer, Automation of next-to-leading order computations in QCD: The FKS subtraction, J. High Energy Phys. 10 (2009) 003.

[24] S. Frixione and B. R. Webber, Matching NLO QCD computations and parton shower simulations, J. High Energy Phys. 06 (2002) 029.

[25] O. B. Bylund, F. Maltoni, I. Tsinikos, E. Vryonidou, and C. Zhang, Probing top quark neutral couplings in the standard model effective field theory at NLO QCD, arXiv:1601.08193.
[26] C. Zhang (to be published).
[27] J. C. Collins, F. Wilczek, and A. Zee, Low-energy manifestations of heavy particles: Application to the neutral current, Phys. Rev. D **18**, 242 (1978).
[28] D. B. Franzosi and C. Zhang, Probing the top-quark chromomagnetic dipole moment at next-to-leading order in QCD, Phys. Rev. D **91**, 114010 (2015).
[29] R. D. Ball, V. Bertone, S. Carrazza, L. Del Debbio, S. Forte, A. Guffanti, N. P. Hartland, and J. Rojo (NNPDF), Parton distributions with QED corrections, Nucl. Phys. **B877**, 290 (2013).
[30] V. Khachatryan *et al.* (CMS Collaboration), Measurement of the t-channel single-top-quark production cross section and of the $|V_{tb}|$ CKM matrix element in pp collisions at $\sqrt{s} = 8$ TeV, J. High Energy Phys. 06 (2014) 090.
[31] ATLAS Collaboration, Measurement of the Inclusive and fiducial cross-section of single top-quark *t*-channel events in pp collisions at $\sqrt{s} = 8$ TeV, (2014).
[32] CMS Collaboration, Combination of cross-section measurements of associated production of a single top-quark and a W boson at sqrt[s] = 8 TeV with the ATLAS and CMS experiments (2014).
[33] B. Schoenrock, E. Drueke, B. A. Gonzalez, and R. Schwienhorst, Single top quark cross section measurement in the t-channel at the high-luminosity LHC, in Community Summer Study 2013: Snowmass on the Mississippi (CSS2013) Minneapolis, MN, USA, July 29–August 6, 2013, arXiv:1308.6307.
[34] M. Selvaggi, Perspectives for top quark physics at high-luminosity LHC, arXiv:1512.04807.
[35] N. Kidonakis, NNLL threshold resummation for top-pair and single-top production, Phys. Part. Nucl. **45**, 714 (2014).
[36] G. Aad *et al.* (ATLAS Collaboration), Search for *s*-channel single top-quark production in proton-proton collisions at $\sqrt{s} = 8$ TeV with the ATLAS detector, Phys. Lett. B **740**, 118 (2015).
[37] CMS Collaboration, Measurement of the W boson helicity using $t\bar{t}$ events in the dilepton final state at sqrt(s) = 8 TeV (2015).
[38] M. Fischer, S. Groote, J. G. Korner, M. C. Mauser, and B. Lampe, Polarized top decay into polarized $Wt(\uparrow) \to W(\uparrow) + b$ at $O(\alpha_s)$, Phys. Lett. B **451**, 406 (1999).
[39] J. de Blas, M. Chala, and J. Santiago, Renormalization group constraints on new top interactions from electroweak precision data, J. High Energy Phys. 09 (2015) 189.
[40] T. Sjostrand, S. Mrenna, and P. Z. Skands, PYTHIA 6.4 physics and manual, J. High Energy Phys. 05 (2006) 026.
[41] P. Artoisenet, R. Frederix, O. Mattelaer, and R. Rietkerk, Automatic spin-entangled decays of heavy resonances in Monte Carlo simulations, J. High Energy Phys. 03 (2013) 015.
[42] G. Aad *et al.* (ATLAS Collaboration), Comprehensive Measurements of *t*-Channel Single Top-Quark Production Cross Sections at $\sqrt{s} = 7$ TeV with the ATLAS Detector, Phys. Rev. D **90**, 112006 (2014).
[43] CMS Collaboration, Single top t-channel differential cross section at 8 TeV, 2014.
[44] Q.-H. Cao, B. Yan, J.-H. Yu, and C. Zhang, A general analysis of Wtb anomalous couplings, arXiv:1504.03785.
[45] K. Hsieh, K. Schmitz, J.-H. Yu, and C. P. Yuan, Global analysis of general $SU(2) \times SU(2) \times U(1)$ models with precision data, Phys. Rev. D **82**, 035011 (2010).
[46] Q.-H. Cao, Z. Li, J.-H. Yu, and C. P. Yuan, Discovery and identification of W' and Z' in $SU(2) \times SU(2) \times U(1)$ models at the LHC, Phys. Rev. D **86**, 095010 (2012).
[47] G. Cacciapaglia, A. Deandrea, D. Harada, and Y. Okada, Bounds and decays of new heavy vector-like top partners, J. High Energy Phys. 11 (2010) 159.
[48] J. A. Aguilar-Saavedra, R. Benbrik, S. Heinemeyer, and M. Perez-Victoria, Handbook of vectorlike quarks: Mixing and single production, Phys. Rev. D **88**, 094010 (2013).
[49] B. Grzadkowski and W. Hollik, Radiative corrections to the top quark width within two Higgs doublet models, Nucl. Phys. **B384**, 101 (1992).
[50] A. Dabelstein, W. Hollik, C. Junger, R. A. Jimenez, and J. Sola, Strong supersymmetric quantum effects on the top quark width, Nucl. Phys. **B454**, 75 (1995).
[51] J.-j. Cao, R. J. Oakes, F. Wang, and J. M. Yang, Supersymmetric effects in top quark decay into polarized *W* Boson, Phys. Rev. D **68**, 054019 (2003).
[52] C.-S. Li, J.-M. Yang, and B.-Q. Hu, Supersymmetric QCD contributions to the top width, Phys. Rev. D **48**, 5425 (1993).
[53] C. Degrande, J. M. Gerard, C. Grojean, F. Maltoni, and G. Servant, Probing Top-Higgs non-standard interactions at the LHC, J. High Energy Phys. 07 (2012) 036.
[54] C. Grojean, E. E. Jenkins, A. V. Manohar, and M. Trott, Renormalization group scaling of Higgs operators and $\Gamma(h \to \gamma\gamma)$, J. High Energy Phys. 04 (2013) 016.
[55] C.-Y. Chen, S. Dawson, and C. Zhang, Electroweak effective operators and Higgs physics, Phys. Rev. D **89**, 015016 (2014).
[56] J. Elias-Mir, C. Grojean, R. S. Gupta, and D. Marzocca, Scaling, and tuning of EW and Higgs observables J. High Energy Phys. 05 (2014) 019.
[57] S. Jung, P. Ko, Y. W. Yoon, and C. Yu, Renormalization group-induced phenomena of top pairs from four-quark effective operators, J. High Energy Phys. 08 (2014) 120.
[58] C. Englert and M. Spannowsky, Effective Theories and measurements at colliders, Phys. Lett. B **740**, 8 (2015).
[59] C. Zhang, Top couplings and new physics: theoretical overview and developments, in 7th International Workshop on Top Quark Physics (TOP2014) Cannes, France, September 28–October 3, 2014, arXiv:1411.7685.
[60] J. D. Wells and Z. Zhang, Renormalization group evolution of the universal theories EFT, arXiv:1512.03056.
[61] C. Hartmann and M. Trott, On one-loop corrections in the standard model effective field theory; the $\Gamma(h \to \gamma\gamma)$ case, J. High Energy Phys. 07 (2015) 151.
[62] C. Hartmann and M. Trott, Higgs Decay to Two Photons at One Loop in the Standard Model Effective Field Theory, Phys. Rev. Lett. **115**, 191801 (2015).